Effects of Possible Scan Geometries on the Accuracy of Satellite Measurements of Water Vapor

LARRY M. MCMILLIN

National Environmental Satellite, Data and Information Service, Office of Research and Applications, Climate Research and Applications Division, Washington, D.C.

MURTY G. DIVAKARLA

Research and Data Systems Corporation, Greenbelt, Maryland

(Manuscript received 15 June 1998, in final form 4 January 1999)

ABSTRACT

For future satellite instruments, two scan geometries have been proposed: cross-track and conical scanning. With the mixtures of possible instruments, a future sounding suite may consist of all cross track, all conical, or a combination with temperature channels on one and moisture channels on the other. This paper evaluates the effect of scan angle on the accuracy of moisture soundings. It is found that, as the scan angle increases from nadir, the accuracy of the moisture soundings near the surface decreases because less of the surface signal reaches the satellite. At the same time, the accuracy of the upper-level sounding increases because the weighting functions become sharper as the angle increases. If a mixed system is required where the temperature and moisture channels have different scan geometries, the best accuracy is obtained if the temperature channels are on a cross-track scanner. The scan angles also affect the number of measurements that are too cloud contaminated to provide accurate meteorological information. A second study shows that the number of radiances that exceed a given error level increases with scan angle. This results in a decrease in coverage for a conical scanning instrument.

1. Introduction

There are two scanning geometries being considered for instruments on earth-observing satellites. In one, the satellite scans across the track. In the second, the satellite scans in a conical pattern. In the cross-track scan, the weighting functions and the polarization change with scan angle. Surface emissivities in the infrared regions are high, so the change in weighting function with angle is the larger effect. Surface emissivities in the microwave region are smaller, especially over water, so the polarization is a larger effect. In the conical scan, the polarization is constant and the weighting function nearly so. The weighting function shifts because of the Doppler shift of the radiation due to the motion of the satellite. For most channels, the weighting functions are broad with respect to the shift and the effect is insignificant. However, the effect can be large for microwave channels that need to be narrow and centered on line centers to measure the upper atmosphere. Another difference is that in the calibration cycle, a cross-track instrument looks at space, while a conical scanning instrument views space by looking at a mirror. This makes calibration of a conical scanning instrument more difficult. The calibration is of particular concern for long-term trends because, while the mirror can be characterized on the ground, changes that occur in space are not monitored. For retrievals, both configurations have been considered. There is even a consideration of a satellite in which the temperature and moisture channels would have different scanning geometries. Rosenkranz et al. (1997) have discussed these and the effect of microwave scan angle on the accuracy of atmospheric temperature retrievals. Because of the possibility that there might be different scanning geometries for the two measurements, we consider the effects of scanning geometry on moisture retrievals and summarize the effect of scanning geometry on cloud contamination in the appendix.

In order to assess the performance of a new instrument, it is necessary to know the capabilities of the alternatives. An instrument which has been launched on a National Oceanic and Atmospheric Administration satellite (*NOAA-15*) and serves as a prototype for future instruments is the Advanced Microwave Sounding Unit

Corresponding author address: Dr. Larry M. McMillin, National Environmental Satellite, Data and Information Service, Office of Research and Applications, Climate Research and Applications Division, 4700 Silver Hill Road, Stop 9910, Washington, DC 20233-9910. E-mail: lmcmillin@nesdis.noaa.gov

(AMSU), which will be a part of the NOAA–KLM series. It is a 20-channel microwave sounding instrument with two separate radiometers. AMSU-A is used for the production of temperature soundings and consists of channels 1–15. The other radiometer is the AMSU-B, which consists of channels 16–20. Channels 1–4 and 15 of AMSU-A and channel 16 and 17 of AMSU-B are window channels. Later versions of the AMSU-B have come to be known as the Microwave Humidity Sounder (AMSU-B), but there are also some minor changes in the channels. Because we used the AMSU-B channel frequencies, we will use that name. Channels 5–14 are all temperature sounding channels with weighting functions spanning the troposphere (channels 5–8) and stratosphere (channels 9–14). Channels 18–20, which are centered on the water vapor line at 183.31 GHz, are the prime channels for humidity profile retrievals. Details of the AMSU channels and their characteristics are given in Table 1.

Results in this paper are shown for cases over both land and water using a model for cloud-free atmospheres developed by Rosenkranz (1993). In the microwave region, the differences can be large due to the low emissivity of water in this region. Over land, the emissivities were calculated using the two-parameter model of Mugnai and Smith (1988) with a soil moisture of 10%. The emissivity changes with soil type and ranges from near unity for dry soils to less than 0.6 for wet soils (Wang and Schmugge 1980; Schmugge 1985; Grody 1988). Other factors such as surface roughness and vegetation contribute to the variability (Owe et al. 1988). Since we used emissivities near unity, the atmospheres over land are observed with a warm background. Over water, the emissivity is rather low (near 50%) and varies with frequency, polarization, incidence angle, sea surface temperature, roughness, and salinity (Lane and Saxton 1952; Ulaby et al. 1986; Sasaki et al. 1987; Rosenkranz 1992). For simulations over water surfaces, a salinity of 36.5 psu and a wind speed of 5 m s^{-1} was assumed. The seawater dielectric constant was estimated using the model developed by Klein and Swift (1977). We selected this model based because it had been verified up to 85 GHz (Rosenkranz 1992), but more recent work (Guillou 1998) suggests that a more accurate model may now be available. The emissivity of the water surface was obtained by averaging the emissivities for the vertical and horizontal polarizations using the Fresnel reflection coefficients given by Ulaby et al. (1986). The model developed by Wisler and Hollinger (1977) was used to account for the emissivity change due to the effects of wind on the sea surface. As expected, the simulations over water have higher reflectivities than simulations over land. The higher reflectivity at the surface increases the contribution of the atmosphere to the measurement because the portion that is reflected has passed through the atmosphere twice. In addition, the portion that is reflected is viewed against a background of cold space, thus increasing the temperature contrast between a given layer of the atmosphere and the radiation entering the layer. Because of these differences, the comparisons were made over both surfaces. Since the measurements over water should contain a greater contribution from the atmosphere, retrieval accuracies should be better over water than over land. Microwave moisture retrievals over water should also be more accurate than infrared moisture retrievals over water for the same reason. The next sections demonstrate this using simulated radiances.

2. Background

The transmittance of an absorbing gas is largely determined by the relation

$$\tau = e^{(-ku)}, \tag{1}$$

where τ is the transmittance, k is the absorption coefficient (which can have weak dependence on pressure, temperature, and gas concentration), and u is the absorber amount. Since k is nearly constant, the value of τ is largely determined by the value of u. When τ is used in the radiative transfer equation given by

$$R = R_s\tau_s\epsilon_s + \int_{\tau_s}^{1} B\, d\tau + (1.0 - \epsilon_s)\tau_s R_{\text{down}}, \tag{2}$$

where R is the radiance observed at the location of the satellite, R_s is the radiance emitted by the surface, τ_s is the transmittance from the surface to space, ϵ_s is the surface emissivity, B is the radiance emitted by the layer of width $d\tau$, and R_{down} is downward radiation at the surface, then the value of R is largely determined by the region where τ is changing most rapidly. Note also that while angle is not explicitly included in Eq. (2) both τ and ϵ are functions of the scan angle. The region of rapid change in τ is determined by the rate of increase of u with pressure and tends, to a first approximation, to occur at a fixed value of u since k is nearly constant. This effect is demonstrated in Fig. 1, which shows the weighting function of two of the water vapor channels expressed as a function of the amount of precipitable water for the tropical and midlatitude profiles shown in Fig. 2. The polar profile is not shown in Fig. 1 because the total water amount is too small to be more than a dot on the vertical axis. The figure demonstrates that the value of R is largely determined by the temperature (or radiance) of the atmosphere at the level where u is equal to a fixed value. For gases with a constant mixing ratio, the value of u corresponds to a given height, once the angle is determined. In this case, the value of u corresponds to a fixed pressure, so it is common practice to label weighting functions that are actually generated at fixed values of u with the corresponding pressure. For gases with a variable mixing ratio, the radiance R is converted to a brightness temperature, then compared to a profile of temperatures or brightness temperatures to determine the height represented by the value of R.

TABLE 1. AMSU channel characteristics.

Channel number	Frequency (GHz)	Bandwidth (MHz)	NEΔT	Pressure at peak of the temperature weighting function
1	23.800	270	0.3	Surface
2	31.400	180	0.3	Surface
3	50.300	180	0.4	Surface
4	52.800	400	0.25	Surface
5	53.596 $\pm$ 0.115	170	0.25	700 mb
6	54.4	400	0.25	400 mb
7	54.94	400	0.25	270 mb
8	55.5	330	0.25	180 mb
9	57.290344 (= fg)	330	0.25	180 mb
10	fg $\pm$ 0.217	78	0.4	50 mb
11	fg $\pm$ 0.3222 $\pm$ 0.048	4*36	0.4	25 mb
12	fg $\pm$ 0.3222 $\pm$ 0.022	4*16	0.6	12 mb
13	fg $\pm$ 0.3222 $\pm$ 0.01	4*8	0.8	5 mb
14	fg $\pm$ 0.3222 $\pm$ 0.0045	4*3	1.2	2 mb
15	89.0	6000	0.5	Surface
16	89.0	6000	0.6	Surface
17	150.0	4000	0.6	Surface
18	183.31 $\pm$ 1.0	1000	0.8	440 mb
19	183.31 $\pm$ 3.0	2000	0.8	600 mb
20	183.31 $\pm$ 7.0	2000	0.8	800 mb

Since the value of u that corresponds to the brightness temperature is known for any given channel, it is the height of the weighting function that changes with water vapor. In other words, the measurement of a water vapor channel represents the temperature at the level where the water vapor along the path from the point to the observer reaches a fixed amount of precipitable water, not a given pressure, and it is the height (pressure) of the weighting function for that channel that represents the changes in the water vapor profile.

This effect is further illustrated by Figs. 2 and 3. Figure 2 shows the temperature and mixing ratio profiles for the tropical, midlatitude, and polar profiles used in Figs. 3 and 4 and the two profiles used in Fig. 1. Note the large change in the values of the mixing ratio. The values for the polar atmosphere are very close to zero. Figure 3 shows the weighting functions (derivatives of the transmittance with respect to pressure) for two moisture channels for the three profiles. For the tropical profile, both channels peak in the upper atmosphere: chan-

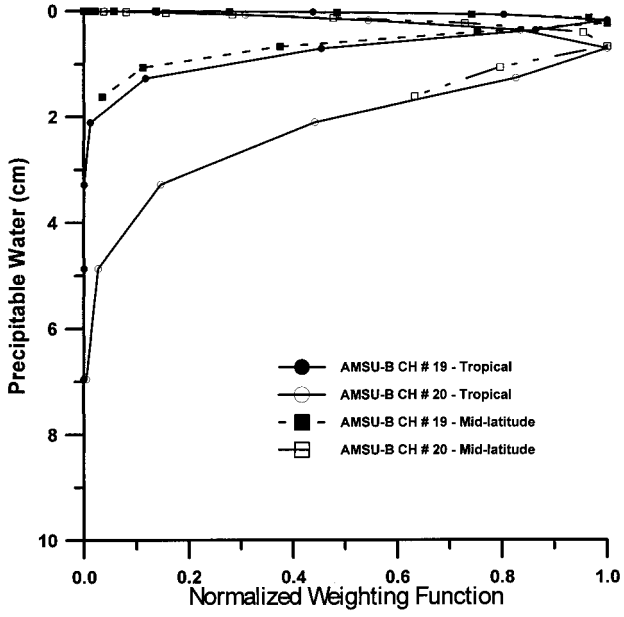

FIG. 1. Weighting functions for tropical and midlatitude profiles for water vapor channels with water vapor as the independent variable.

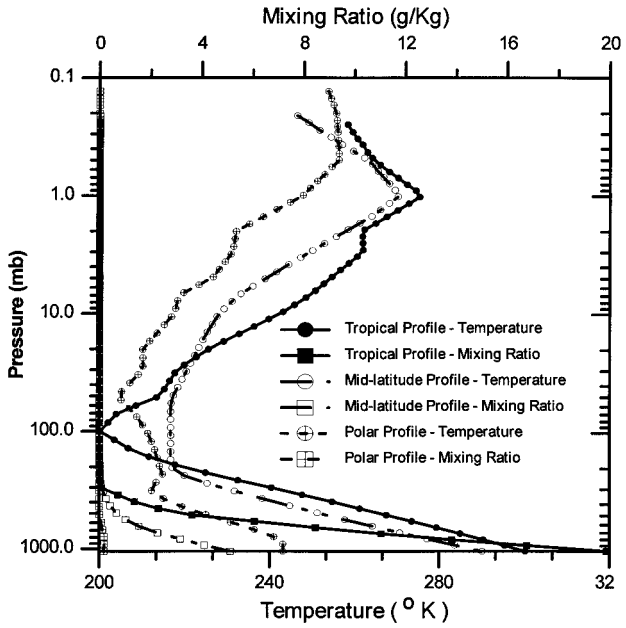

FIG. 2. Temperature and moisture profiles for the tropical, midlatitude, and polar atmospheres.

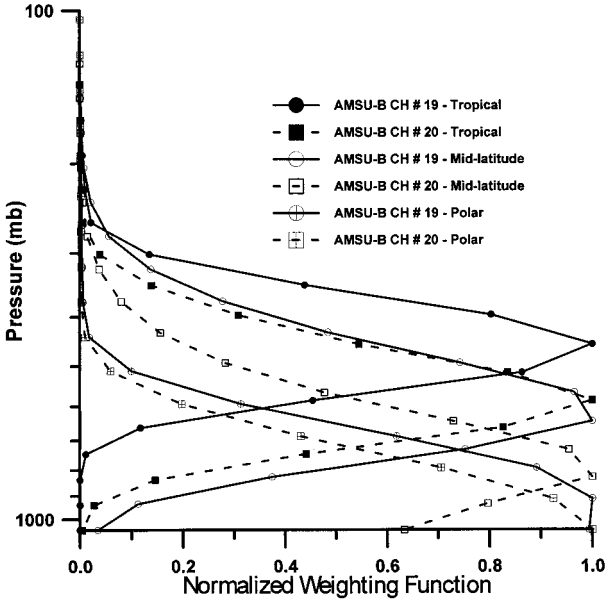

FIG. 3. Weighting functions with pressure as the independent coordinate for two channels for the tropical, midlatitude, and polar atmospheres shown in Fig. 2.

nel 19 near 400 mb and channel 20 near 600 mb. For the midlatitude profiles, channel 19 peaks near 600 mb and channel 20 peaks near 800 mb. For the polar atmosphere, both become surface channels. Figure 4 illustrates the change in weighting function that occurs as a result of a change in angle. Note that the upward shift in the upper wing of the weighting function is less than the upward shift in the bottom wing. Because the upward shift in the lower wing is larger, the weighting functions become narrower as they shift to higher elevations.

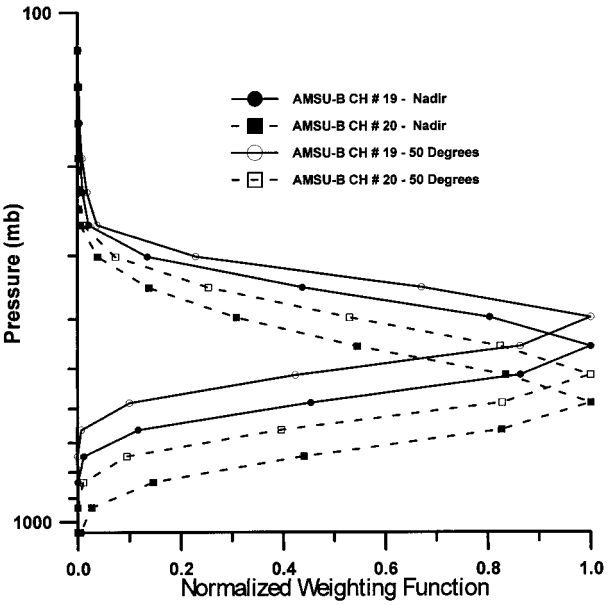

FIG. 4. Weighting functions for two channels at nadir and at 50° for a tropical atmosphere.

TABLE 2. Distribution of the profiles in the training dataset over water.

Latitude	Jan–Mar	Apr–Jun	Jul–Sep	Oct–Dec	Total
90°–60°N	38	67	68	28	201
60°–30°N	96	137	132	105	470
30°N–30°S	179	135	109	138	561
30°–60°S	161	85	50	124	420
60°–90°S	36	16	4	29	85
Total	510	440	363	424	1737

3. Data description and analysis procedure

The results in this study are based on simulated brightness temperatures and a standard regression retrieval. The atmospheres used to simulate microwave brightness temperatures were taken from a radiosonde–rocket collocated dataset. The rocket data were appended to radiosondes above 100 mb to obtain profiles of temperature and moisture up to 0.1 mb (M. Goldberg 1998, personal communication). There are two datasets: one for 1989, and the other for 1988. From the 1989 dataset, 1737 profiles over water were selected and used as a training dataset. The distribution of the profiles in the training dataset over water as a function of latitude and month is shown in Table 2. Table 3 shows the distribution for the 569 profiles that were selected as an independent set from the 1988 data. Table 4 shows the distribution for the 1661 profiles in the training dataset over land, and Table 5 shows the distribution for the 1431 profiles in the independent set.

The microwave brightness temperature calculations were performed at the AMSU frequencies using the transmittance (Rosenkranz 1993) and surface models (various authors) discussed in the introduction. Attenuation due to ozone and other minor constituents and the contribution of background cosmic radiation were neglected. The dependent data were used to generate regression coefficients using the equation

$$\mathbf{C} = \mathbf{X}\mathbf{T}^{*\mathrm{T}}(\mathbf{T}^{*}\mathbf{T}^{*\mathrm{T}})^{-1}, \tag{3}$$

where $\mathbf{C}$ is the level by channel matrix of regression coefficients, $\mathbf{X}$ is level by observation matrix of the

TABLE 3. Distribution of the profiles in the independent dataset over water.

Latitude	Jan–Mar	Apr–Jun	Jul–Sep	Oct–Dec	Total
90°–60°N	12	5	36	8	61
60°–30°N	35	5	35	11	86
30°N–30°S	86	27	79	23	215
30°–60°S	81	16	59	11	167
60°–90°S	35	4	1	0	40
Total	249	57	210	53	569

TABLE 4. Distribution of the profiles in the training dataset over land.

Latitude	Jan–Mar	Apr–Jun	Jul–Sep	Oct–Dec	Total
90°–60°N	137	116	85	95	433
60°–30°N	144	83	70	96	393
30°N–30°S	193	102	131	98	524
30°–60°S	97	51	55	51	254
60°–90°S	37	10	1	9	57
Total	608	362	342	349	1661

TABLE 5. Distribution of the profiles in the independent dataset over land.

Latitude	Jan–Mar	Apr–Jun	Jul–Sep	Oct–Dec	Total
90°–60°N	81	42	141	38	302
60°–30°N	171	38	140	86	435
30°N–30°S	174	33	133	62	402
30°–60°S	122	21	76	34	253
60°–90°S	31	3	5	0	39
Total	579	137	495	220	1431

quantities being retrieved (temperature or water vapor), and $\mathbf{T}^*$ denotes the channel by observation matrix of brightness temperatures including noise. The magnitude of the noise was set to the expected instrumental value for the given channel. The retrieval is then given by

$$\mathbf{X} = \mathbf{C}\mathbf{T}^*. \tag{4}$$

The AMSU-A temperature channels were used for the temperature regression. The moisture channels provide little information for the temperature retrievals because the uncertainty in the height of the measurement acts as noise for the temperature retrieval. If they are used, there is a slight (0.1 K near the surface and at 400–500 mb) increase in accuracy. For moisture retrievals, all of the channels from both the AMSU-A and AMSU-B instruments are needed and were used. Regression coefficients were applied to the brightness temperatures simulated using an independent dataset to retrieve temperature and moisture profiles. The rms errors were calculated for the temperature and moisture at each pressure level.

In order to compare results, a measure of performance is required. This is easy for temperature, but water vapor is not easily characterized by a standard deviation over a sample because of the large range of water vapor values. If one uses mixing ratio, a relatively small error in a moist tropical profile can far exceed the total water vapor in a dry polar atmosphere. If profiles are mixed, the standard deviation will represent the accuracy of only the tropical profiles; the polar profiles will be lost in the noise. If one reports relative humidity, a similar problem occurs, but in reverse. In a cold atmosphere the saturation vapor pressure approaches zero, and the relative humidity becomes the ratio of two small numbers. When the relative humidity is calculated from mixing ratios, the errors in the relative humidity can be large. When statistics are calculated, a few large errors from the cold atmosphere can dominate the statistics. We chose to represent the moisture accuracy as a percentage of the true value. This has the same numerical problems as the relative humidity, but we solve the problem by screening out the profiles with very low humidity.

When evaluating water vapor retrieval algorithms, one has to be aware that moisture is, to a very large extent, determined by the atmospheric temperature. This dependence exists because the saturation mixing ratio is determined by the temperature. This also means that there is an accuracy to which the water vapor can be determined from the temperature channels without any moisture channels. We use this accuracy as a given and rate the improvement in water vapor retrieval accuracy relative to this value, rather than a climatological mean value. This is a much tougher but more realistic test. It is easy to generate retrievals that look good compared to a climatological mean but poor compared to the moisture estimate obtained from the temperature channels. Moisture channels add information, but the marginal gain in accuracy is smaller than many people expect. We give this result, not as a proposed method, but as a reference value to be used to measure the actual information provided by the moisture channels.

4. Results and discussion

The accuracy of the moisture information that can be obtained from the temperature channels alone is shown in Figs. 5 and 6. These figures compare the retrievals with water vapor channels to those obtained with only

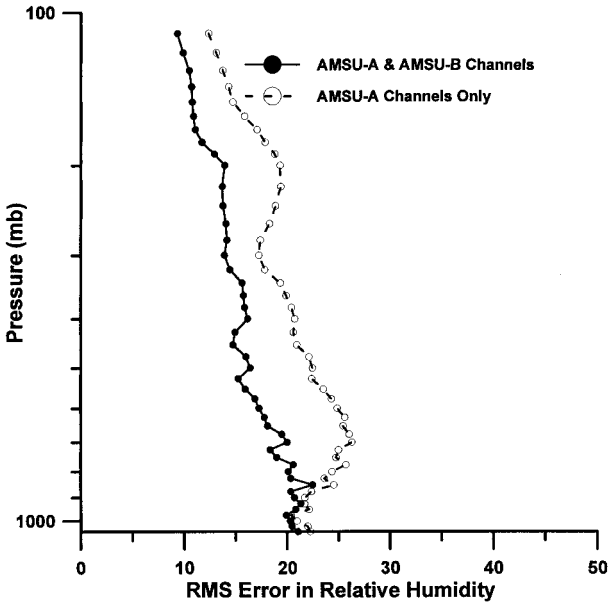

FIG. 5. A comparison of water vapor retrievals from just the temperature channels to water vapor retrievals with temperature and moisture channels over land.

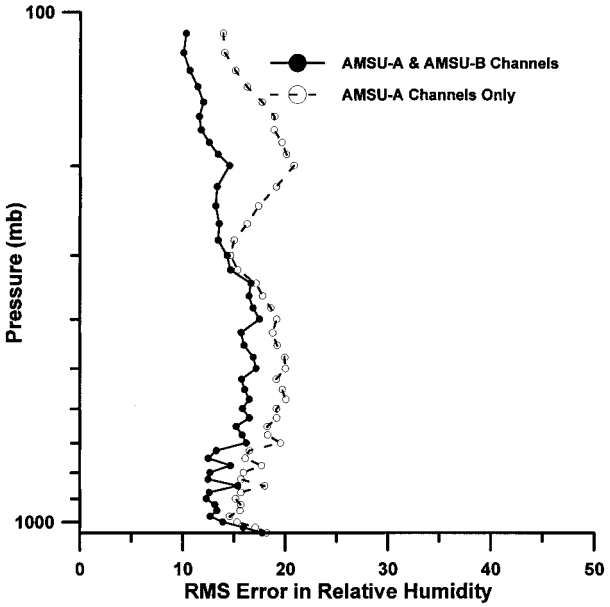

FIG. 6. A comparison of water vapor retrievals from just the temperature channels to water vapor retrievals with temperature and moisture channels over water.

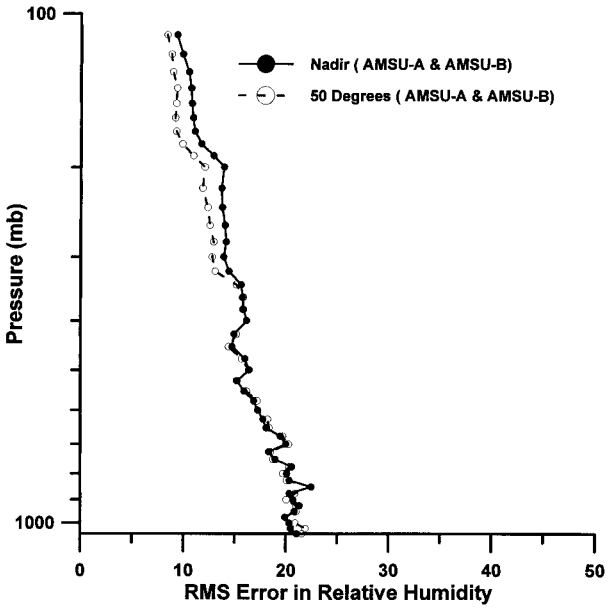

FIG. 7. A comparison of water vapor retrievals at two different viewing angles (nadir and 50°) over land.

the temperature channels. The errors are the result of a retrieval for relative humidity. Predicting the relative humidity was compared to predicting the mixing ratio. The prediction for relative humidity was more accurate, even when the relative humidity predictions were converted to mixing ratios, and the comparison was done on mixing ratios. Figure 5 presents the results over land. The retrieval without the water vapor channels is accurate to about 20%. The accuracy increases to give an error of 10%–15% with the water vapor channels. It is also interesting to note that, at the surface, the errors are almost identical. The moisture channels help in the middle atmosphere. This may be a reflection of the fact that the moisture channels need a temperature contrast to provide moisture information. That is, the brightness temperature of the radiation entering a layer must differ from the temperature of the layer if the amount of water vapor is to affect the measured radiation. Near the surface this contrast is low, especially at night over land where temperature inversions near the surface are common. It may also reflect the importance of the surface temperature in establishing the vapor pressure near the ground. Figure 6 gives the equivalent results over water. Over water, the results show a similar pattern, but the retrievals are more accurate. The prediction from the temperature channels varies between 15% and 20% for the troposphere and is about 18% at the surface. When all the channels are used, the error reduces to about 15% for most of the troposphere and 17% at the surface. The remaining comparisons were done using all the AMSU-A and AMSU-B channels to predict moisture.

A major objective of this study was to determine the effect of scan angle on moisture retrieval accuracy. As mentioned earlier, at a higher scan angle, the transmittance of a channel spans a given range of absorber amount in less vertical space. As a result, the weighting function is lifted and narrowed. The narrowing is most obvious in the limit as the weighing function lifts to its maximum and the instrument becomes a limb sounder. The results of these effects are shown in Fig. 7 for land and Fig. 8 for water. The general trend in both figures is for better retrieval accuracy near the surface for the

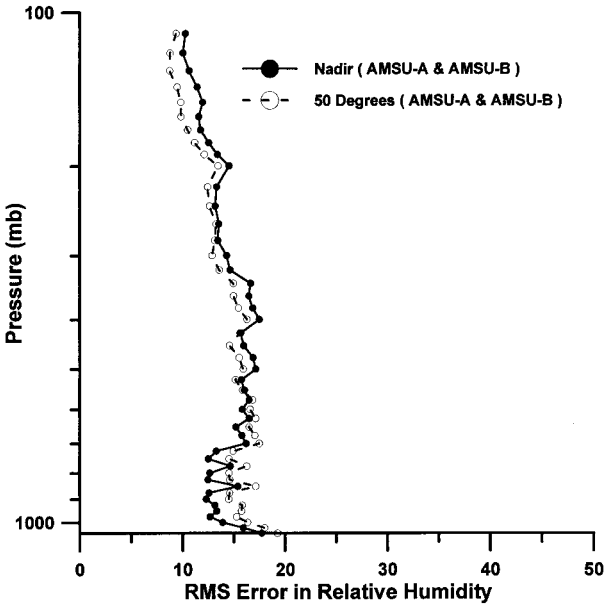

FIG. 8. A comparison of water vapor retrievals at two different viewing angles (nadir and 50°) over water.

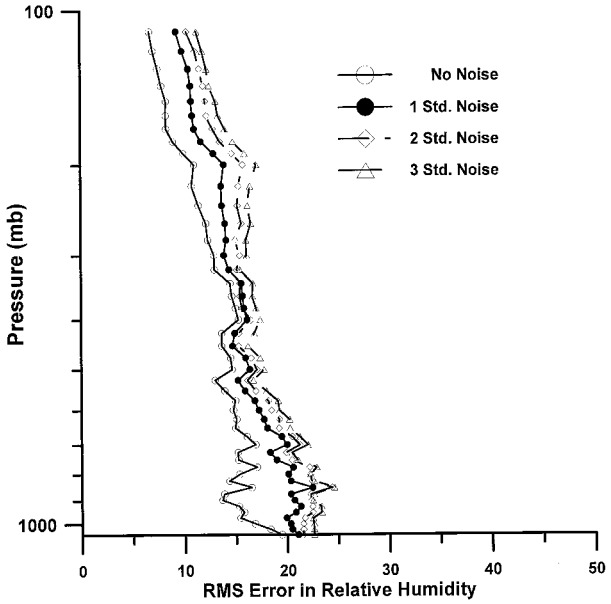

FIG. 9. Water vapor retrieval accuracy as a function of noise over land at nadir.

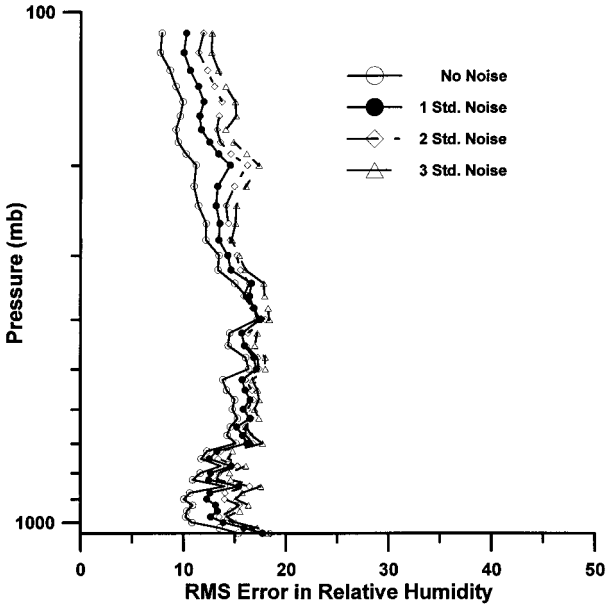

FIG. 10. Water vapor retrieval accuracy as a function of noise over water at nadir.

nadir scanner, but the effect is greater over the ocean. The increase in accuracy near the surface occurs because the channels are most transparent at nadir and the response to the surface is maximized. It is largest for the ocean case because the surface emissivity increases the sensitivity to the lower atmosphere. Near 600 mb, the situation reverses and the retrievals at 50° become more accurate. This is due to the narrowing of the weighting functions, which increases the vertical resolution.

The interest in the effect of the scan angle arose from the possibility that, at some time in the future, it may be necessary to use moisture channels on a conical scanning instrument with temperature data from either a forecast or a cross-track scanner. In such a case, the different source of the temperature data becomes a contributor to the noise budget. Figures 9 and 10, again for land and water, show the retrieval accuracy as a function of the noise. The noise of the AMSU shown in Table 1 serves as the standard noise. Accuracies are shown for the cases of no noise, and one, two, and three times the standard noise level. Clearly, a substantial gain in accuracy is possible if the noise can be reduced. Again, the most accurate results are obtained over water. Both the level of the noise and the spread are higher over land than over water. Reducing the noise has the largest effect on the least accurate results.

When scan geometries are mixed, it is possible either to adjust the moisture channels to simulate the scan geometry of the temperature channels or to adjust the temperature channels to the scan geometry of the moisture channels. In either case the adjustment causes an increase in the noise of the adjusted component. Figures 11–14 show the result of increasing the noise of just the temperature channels or just the moisture channels. Figures 11 and 12 show the effect of the noise in the AMSU-B channels over land and ocean. There is the usual improvement in retrieval accuracy over water. From 300 to 100 mb, there is a significant dependence on noise. The noise has little effect near the surface. Figures 13 and 14 show the effect of noise in the AMSU-A channels. In contrast to the previous example, decreasing the noise has a large effect near the surface

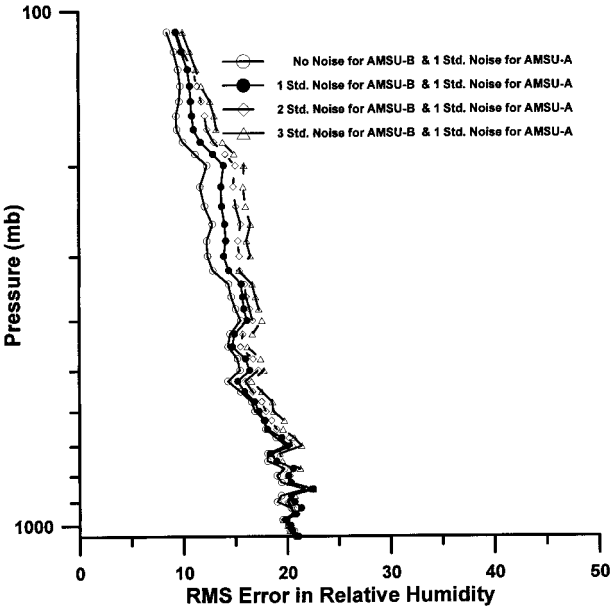

FIG. 11. Water vapor retrieval accuracy as a function of noise in the AMSU-B channels over land at nadir.

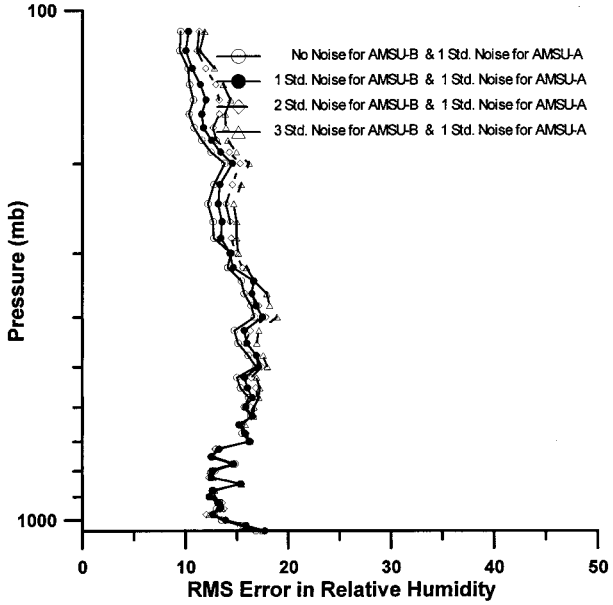

FIG. 12. Water vapor retrieval accuracy as a function of noise in the AMSU-B channels over water at nadir.

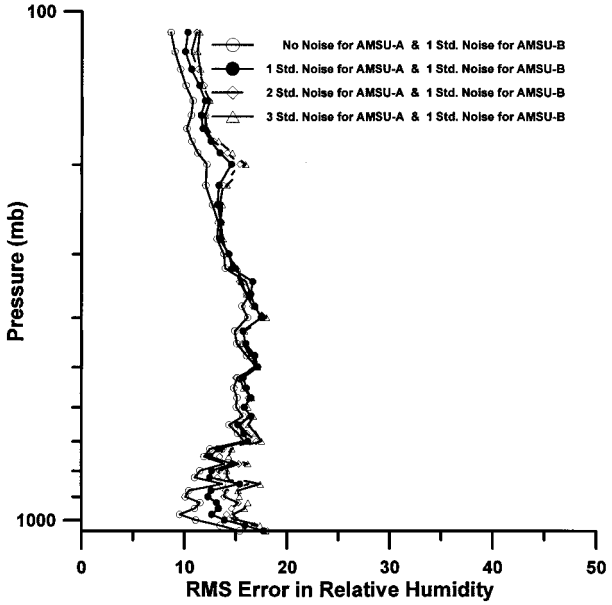

FIG. 14. Water vapor retrieval accuracy as a function of noise in the AMSU-A channels over water at nadir.

and a relatively small effect above 500 mb. These figures suggest that the best configuration depends on the region that is important. The noise in the AMSU-A channels is important near the surface, while the noise in the AMSU-B channels is important for the upper atmosphere.

Figures 15 and 16 compare the results for a nadir-viewing instrument with an instrument in which the moisture channels are at nadir and the temperature channels are at 50°. When such an angle adjustment is made to match the observations, several additional errors are introduced. Among these are the error in the adjustment and the error in the collocation adjustment. If these errors are known, the previous figures can be used to make an adjustment. For Figs. 15 and 16, these errors were assumed to be negligible. Over land there is little difference as the temperature channels are changed from nadir to 50°, but over water, the decrease in accuracy

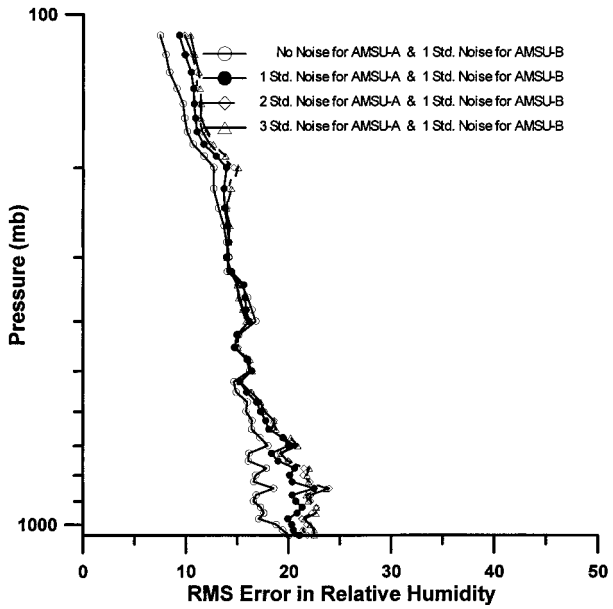

FIG. 13. Water vapor retrieval accuracy as a function of noise in the AMSU-A channels over land at nadir.

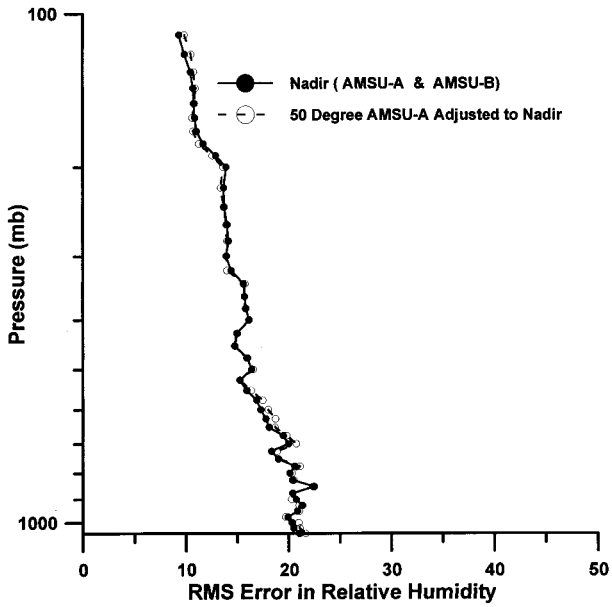

FIG. 15. Effect of angle for the AMSU-A on nadir water vapor retrieval accuracy over land.

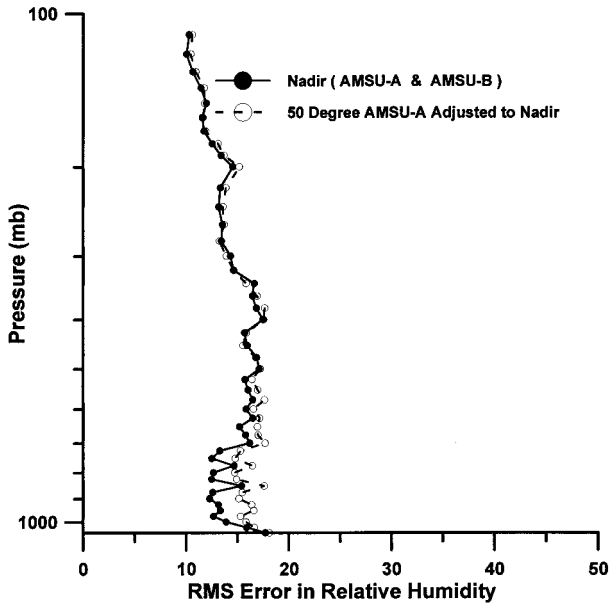

FIG. 16. Effect of angle for the AMSU-A on nadir water vapor retrieval accuracy over water.

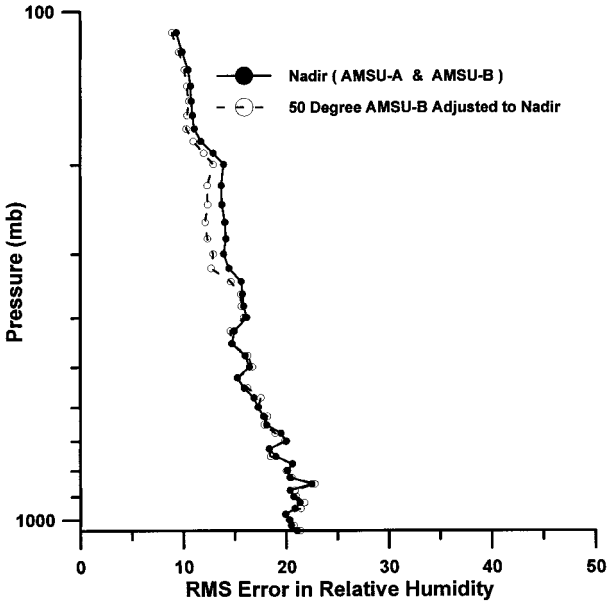

FIG. 17. Effect of angle for the AMSU-B on nadir water vapor retrieval accuracy over land.

is about 3.5% (from 16% to 12.5%) near the surface. The alternative case, where the moisture channels are adjusted to nadir, is shown in Figs. 17 and 18. In this configuration, there is little difference near the surface and a slight increase in accuracy at the upper levels. These results suggest that placing the moisture channels on a different scan geometry makes little difference in the retrieval accuracy. This is consistent with the previous result that the error in the moisture channels does not have as large an effect on the accuracy as an error in the temperature channels.

An effect that has not been explicitly discussed is the effect of scan angle on the number of observations. Larger angles mean longer paths through error sources such as clouds. The effect of scan angle on error was investigated in another study that is presented as an appendix. The major conclusion is that the number of observations for which clouds cause errors that exceed a given limit increases as the scan angle increases. It is better to scan in the nadir direction to avoid cloud contamination.

5. Summary and conclusions

This study was designed to provide an evaluation of the effect of various options for the design of a microwave instrument. The major conclusions are as follows.

1) There is potential for a significant increase in accuracy if the noise level can be reduced.
2) Increasing the scan angle decreases the accuracy of water vapor retrievals at lower levels, but increases it at upper levels.
3) Because of the strong relationship between temperature and the saturation vapor pressure, the temperature channels have a large impact on the moisture retrieval accuracy.
4) If cloud effects are ignored, placing the moisture channels on an instrument with a large scan angle has little effect on retrieval accuracy.
5) Cloud contamination increases as the pathlength increases in clouds, and a higher scan angle produces more contamination that results in larger errors.

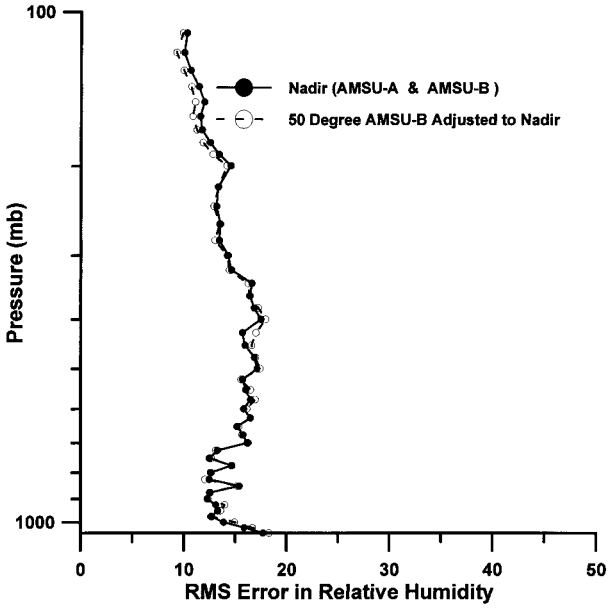

FIG. 18. Effect of angle for the AMSU-B on nadir water vapor retrieval accuracy over water.

Acknowledgments. The research reported in this paper was supported by the Integrated Program Office as part of an internal concept study of using an interferometer for the infrared sounder in the National Polar-Orbiting Operational Environmental Satellite System. One of the reviewers provided many helpful suggestions.

APPENDIX

Cloud Contamination in Cross-Track and Conical Scanning Configurations

One of the more important effects of the scan geometry is the difference in the number of soundings obscured by clouds. It is clear that, as the angle increases, the path through the clouds becomes longer. This diminishes the number of spots that can be used either for retrievals or to cloud clear the high-resolution infrared sounder data. To quantify this effect, an evaluation of the effect of cloud liquid water on microwave sounding channels was performed for two view angles (0° and 60°) to infer cloud contamination in cross-track and conical instrument configurations.

The effect of the upward shift in weighting function as a function of view angle on the (cloudy–clear) brightness temperature depends on the channel. Channels that sense the surface are affected most; channels that peak above both the clouds and the surface are relatively unaffected. To prevent this effect from biasing the conclusions, we simulated typical effects by selecting two channels in which weighting functions are similar in that they sense the same height when viewing at two different angles. Our selected channels are channel 5 (53.596 GHz) at 0° (nadir) and channel 4 (52.8 GHz) at 60°. Another set of weighting functions are channel 6 (54.5 GHz) at 0° (nadir) and channel 5 at 60° modified to 53.76 GHz to more closely match the height of channel 6. To quantify the effect of cloud contamination in cross-track and conical scanning modes, simulations were performed for these channels at 0° and 60° view angles. Note that 60° is slightly larger than the 53° angle used for current conical instruments, but the exact angle that might be used on future instruments is not known because the scan angle is a compromise of conflicting optimizations.

The microwave absorption model developed by Rosenkranz (1993) was used for the calculation of absorption due to molecular oxygen and water vapor. For simulations over water, a salinity of 36.5 psu and a wind speed of 5 m s^{-1} were assumed and the emissivity of sea surface was calculated using Fresnel reflection coefficients. For simulations over land, the surface emissivity was calculated based on 10% soil moisture with a two-parameter model (Mugnai and Smith 1988).

To simulate the radiation transfer in cloudy atmospheres, cloud properties (Gaut and Reifenstein 1971) such as cloud height, thickness, and liquid water density for five cloud categories (Cumulus, Cu; Cumulonimbus, Cb; Stratus, St; Nimbostratus/Altostratus/Alsocumulus, Ns/As/Ac; Cirrus, Ci) were used. Cloud fractions from these cloud types were weighted to conform to the global cloud cover distribution over oceans (Warren et al. 1986) and land (Warren et al. 1988). Small cloud droplets that satisfy Rayleigh criteria were assumed and the microwave absorption coefficient of liquid water clouds was approximated by the single-Debye relationship (Grody 1993).

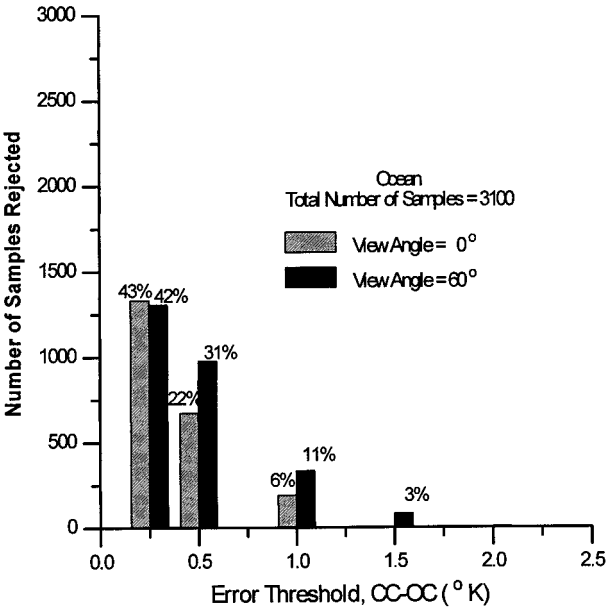

FIG. A1. Total number of samples rejected at 0° and 60° view angles over ocean at different (CC–OC) error threshold values.

Brightness temperatures were calculated for the independent dataset (620 atmospheric profiles over ocean and 290 profiles over land) for cloud-free [Observed Clear (OC)] and cloud-contaminated radiances. The cloud contaminated values were then adjusted to give corrected clear (CC) values. The cloud adjustment was done using standard regression to predict the clear values. The predictor was the cloudy value for the given channel, so the correction consisted of a single slope and a single intercept for each channel. The regression coefficients were derived from a sample of simulated radiances. The difference between the CC and OC values was then calculated. Using different (CC − OC) errors as a threshold, the number of samples that exceed each error level (0.25, 0.5, 1.0, 1.5, 2.0) for 0° and 60° view angles were obtained for channels 5 and 6. Figures A1 and A2 show the bar graphs of the total number of samples that exceed a given error level and thus are considered to be rejected for atmospheric retrievals. The bar graphs are shown for channel 5 for both the view angles over water and land, respectively. The cloud contamination in channel 6 (not shown in this paper) at both the view angles is similar in trend to channel 5 but is smaller by an order of magnitude. Although these

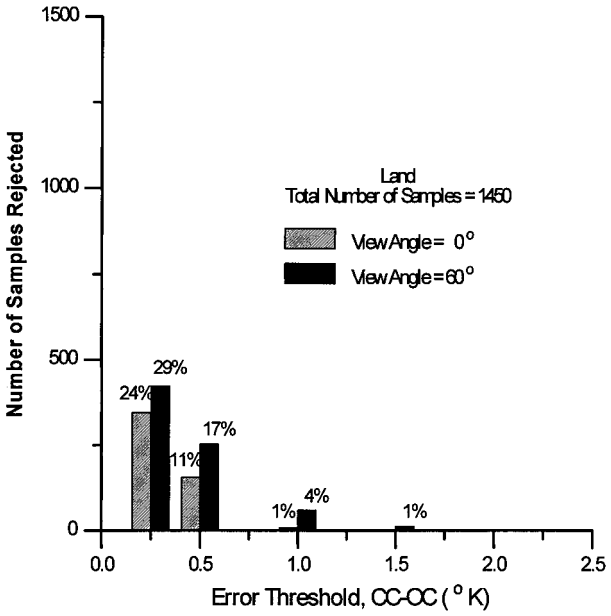

FIG. A2. Total number of samples rejected at 0° and 60° view angles over land at different (CC–OC) error threshold values.

figures depict the overall statistics, statistics from individual cloud types reveal the expected result that the number of rejections due to high- and middle-level clouds (Ci, Ns/As/Ac) is less than the number of rejections from low clouds. However, these clouds (Ns/As/Ac) affect the signal at 60° to a greater degree due to the longer path and increase the number of rejections at 60°.

The number of rejections is also affected by the surface emissivity and its variation. Over water (emissivity $\sim 0.55 \pm 0.05$) the temperature sensed by a microwave instrument takes a value between that of cold space and the surface. Because of the contribution from cold space, a cloud that blocks the view to cold space can produce a warmer temperature than that produced by a clear scene. As the local zenith angle is increased, the path through the atmosphere is increased and the temperature for the clear case typically becomes colder. This means that, for some of these clouds, there can be one angle for which the temperature of a clear area exactly matches the temperature of the cloud. For these cases, the effects cancel. However, for a particular cloud, there is only one channel (atmospheric level) for which the cloud effects cancel. In a retrieval, channels at multiple levels are used. Although the effect can be zero for one channel, it will not be zero for channels that peak at different heights. The overall effect on a sounding is that there will always be some channels that will be cloud contaminated. When all channels are considered, the high-angle observations show a decrease in accepted sample for all conditions because there will be at least one angle that is affected. Over land, where the emissivity is close to unity, the percentage of rejections is far less than those over water. At the 60° view angle, the number of rejections increases due to the longer cloud liquid water path within these clouds. Although the emissivities used over ocean are representative of the variability, the emissivities used over land represent only dry conditions. Results over land can range from the dry values to conditions that are nearly equal to those obtained over oceans for wet soils.

This study shows that the area that exceeds a given level of contamination is larger for a conical scanning than for a cross-track configuration, and that this is true for both land and ocean cases. Even when the numbers of rejections are relatively uniform at an error level of 0.25 K (Fig. 1), the number of samples with large errors (1.5 K) is greater at 60°. It is important to note that, although we speak in terms of samples being rejected, what we really mean is the number that exceed a given error threshold in this ideal case where we know the truth and thus the error. In practice, the spots must be detected by some independent means such as a horizontal consistency check. If they are not detected, the contamination will cause errors in the retrievals.

The results presented here clearly indicate that the longer path through a contaminating cloud in a conical configuration will increase the area obscured by clouds. Surface emissivity and cloud properties play a significant role in deciding the number of rejections at nadir and high view angles. At high angles, the effect of surface emissivity is marginal. The advantage of the cross-track scanner depends on the error limit that is used. At 0.25 K over oceans, the effects are nearly equal. At large error thresholds, the rejection rate for the conical scan is much higher. The final numbers are a function of correction algorithms, retrieval algorithms, and cloud statistics.

REFERENCES

Gaut, N. E., and E. C. Reifenstein, 1971: Interaction model of microwave energy and atmospheric variables. ERT Tech. Rep. 13, 167 pp. [Available from Environmental Research and Technology, Inc., 35 Nagog Park, Acton, MA 01720.]

Grody, N. C., 1988: Surface identification using satellite microwave radiometers. *IEEE Trans. Geosci. Remote Sens.,* **26,** 850–859.

——, 1993: Remote sensing of the atmosphere from satellites using microwave radiometry. *Atmospheric Remote Sensing by Microwave Radiometry,* M. A. Janssen, Ed., John Wiley and Sons, 259–314.

Guillou, C., W. Ellison, L. Eymard, K. Lamkaouchi, C. Prigent, G. Delbos, G. Balana, and S. A. Boukabara, 1998: Impact of new permittivity measurements on sea surface emissivity modeling in microwaves. *Radio Sci.,* **33,** 649–667.

Klein, L. A., and C. T. Swift, 1977: An improved model for the dielectric constant of sea water at microwave frequencies. *IEEE Trans. Antennas Propag.,* **AP-25,** 104–111.

Lane, J. A., and J. A. Saxton, 1952: Dielectric dispersion in pure polar liquids at very high radio frequencies. *Proc. Roy. Soc. London,* **214A,** 531–545.

Mugnai, A., and E. C. Smith, 1988: Radiative transfer to space through a precipitating cloud at multiple microwave frequencies. Part I: Model description. *J. Climate Appl. Meteor.,* **27,** 1055–1073.

Owe, M., A. Change, and R. E. Golus, 1988: Estimating surface soil moisture from satellite microwave measurements and a satellite-derived vegetation index. *Remote Sens. Environ.,* **24,** 331–345.

Rosenkranz, P. W., 1992: Rough-sea microwave emissivities measured with the SSM/I. *IEEE Trans. Geosci. Remote Sens.,* **30,** 1081–1085.

——, 1993: Absorption of microwaves by atmospheric gases. *Atmospheric Remote Sensing by Microwave Radiometry,* M. A. Janssen, Ed., John Wiley and Sons, 37–79.

——, K. D. Hutchinson, K. R. Hardy, and M. S. Davis, 1997: An assessment of the impact of satellite microwave sounder incidence angle and scan geometry on the accuracy of atmospheric temperature profile retrievals. *J. Atmos. Oceanic Technol.,* **14,** 488–494.

Sasaki, Y., I. Asanuma, K. Muneyama, G. Naito, and T. Suzuki, 1987: The dependence of sea-surface microwave emission on wind speed, frequency, incidence angle, and polarization over the frequency range from 1 to 40 GHz. *IEEE Trans. Geosci. Remote Sens.,* **GE-25,** 138–146.

Schmugge, T. J., 1985: Remote sensing of soil moisture. *Hydrological Forecasting,* M. G. Anderson and T. P. Burt, Eds., John Wiley.

Ulaby F. T., R. K. Moore, and A. K. Fung, 1986: Passive microwave remote sensing of the atmosphere. *Microwave Remote Sensing: Active and Passive, Vol. III: From Theory to Applications,* Artech House, 1282–1531.

Wang, J. R., and T. J. Schmugge, 1980: An empirical model for the complex dielectric permittivity of soils as a function of water content. *IEEE Trans. Geosci. Remote Sens.,* **GE-18,** 288–295.

Warren, S. G., C. J. Harn, J. London, R. M. Chervin, and R. Jenne, 1986: Global distribution of total cloud cover and cloud type amounts over ocean. NCAR/TN-317+STR, 212 pp.[Available from National Center for Atmospheric Research, P.O. Box 3000, Boulder, CO 80307.]

——, ——, ——, ——, and ——, 1988: Global distribution of total cloud cover and cloud type amounts over land. NCAR/TN-273+STR, 212 pp. [Available from National Center for Atmospheric Research, P.O. Box 3000, Boulder, CO 80307.]

Wisler M. M., and J. P. Hollinger, 1977: Estimation of marine environmental parameters using microwave radiometric remote sensing systems. NRL Memo. Rep. 3661. [Available from Naval Research Laboratory, 4555 Overlook Ave., Washington, DC 20375.]